Dynamic Article Links ▶

PAPER

Brightly fluorescent red organic solids bearing boron-bridged π–conjugated skeletons†

Di Li,[a] **Kai Wang,**[a] **Shuo Huang,**[a] **Songnan Qu,**[b] **Xingyuan Liu,**[b] **Qingxin Zhu,**[c] **Hongyu Zhang***[a] **and Yue Wang**[a]

Two π-conjugated organoboron complexes **1** and **2** with highly efficient red (632 nm) and deep red (670 nm) solid-state fluorescence have been constructed and qualified as potential non-doped red emitters accompanied by excellent electron-transport ability. X-ray crystal analysis demonstrated that the two side phenyl groups coordinated to each boron atom effectively keep the luminescent units apart. As a result, these red fluorophores are brightly fluorescent in the solid state (fluorescence quantum yields: 0.30 for **1** and 0.41 for **2**). In addition, these boron complexes possess good thermal stability and high electron-transport ability. Organic light-emitting diodes employing **1** or **2** as non-doped emitters with simple device configuration exhibit bright red and near-infared electroluminescence.

Introduction

Highly bright emissive organic solids are urgently in demand for various applications, including organic light emitting diodes (OLEDs), photoelectric conversion, and lasers.[1] Whereas many fluorophores emit strongly when molecularly dissolved in solvents, they become weak fluorophores in the solid state because of aggregation-caused fluorescence quenching. Red fluorescent materials are usually polar in nature or possess an extended π-conjugated structure. Thus, fluorescence quenching is particularly serious for red fluorophores due to either attractive dipole–dipole interactions or effective intermolecular π-stacking. For example, dipolar 4-dicyanomethylene-4*H*-pyran-containing fluorescent dyes or extended acene-series red fluorophores are highly fluorescent in solution but suffer heavy fluorescence quenching in the solid state.[2] In this regard, there is an urgent demand to construct red emissive materials with high solid-state fluorescence efficiency and color purity.

Extended π-conjugated molecules with ring-fused structures have attracted considerable attention since their flat and rigid π-conjugated skeletons bring about a set of desired properties, such as intense luminescence, good thermal stability and high carrier mobility that are important in terms of their applications in high-performance optoelectronics.[3,4] Rigid structures can effectively restrict molecular rotations, which usually cause serious fluorescence quenching and flat π-conjugated skeletons may facilitate charge transport due to intermolecular π-electron delocalization. Four-coordinate boron compounds are a family of efficient emitters in OLEDs and several classes of four-coordinate boron chromophores, including N,O-, N,N- and N,C-chelate π-systems have been designed and synthesized.[5–8] The four-coordinate boron-contained molecules with four-, five- and six-ring fused skeletons have been recently realized, and this synthetic strategy produced bright emitting materials with blue, green, and yellow emission colors.[9–11] However, red fluorescent all-ring-fused molecules containing boron moieties have not yet been achieved due to the difficulty in further extending the π-conjugation.

Recently, Kwak and Kim synthesized BF₂-chelate fluorophores based on 2-(2′-hydroxyphenyl)benzoxazole and 2-(2′-hydroxyphenyl)benzothiazole ligands (Chart 1a, R = F).[11] These boron complexes that have a four-ring fused skeleton emitted bright blue fluorescence. In this contribution, we designed two brightly fluorescent red and deep red boron-containing complexes by extending the π-conjugation (Chart 1b, R = Ph). The rigid π-conjugated framework with side phenyl substitutes endows them with good thermal stability, high electron mobility, and intense solid-state fluorescence. To demonstrate their potential in optoelectronics, charge carrier mobilities as well as electroluminescent (EL) properties have been studied.

[a]State Key Laboratory of Supramolecular Structure and Materials, College of Chemistry, Jilin University, Changchun, 130012, P. R. China. E-mail: hongyuzhang@jlu.edu.cn; Tel: +86-431-85168496

[b]Key Laboratory of Excited State Processes, Changchun Institute of Optics, Fine Mechanics and Physics, Chinese Academy of Sciences, Changchun, 130033, P.R. China

[c]State Key Laboratory of Inorganic Synthesis and Preparative Chemistry, College of Chemistry, Jilin University, Changchun, 130012, P. R. China
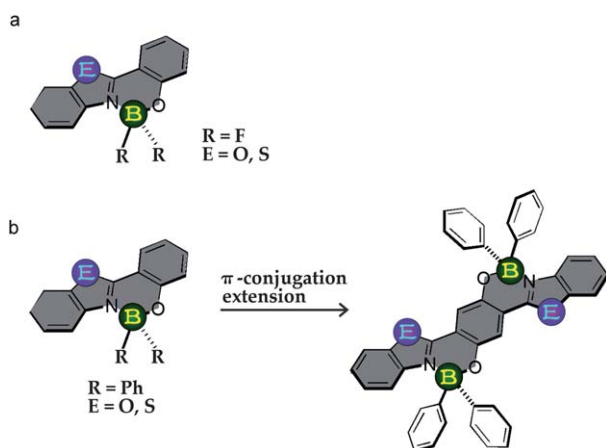
Chart 1 The design strategy towards diboron-containing complexes with a seven-ring fused π-conjugated skeleton.

Experimental section

General information

All starting materials were purchased from Aldrich Chemical Co. and used without further purification. THF was freshly distilled over sodium and benzophenone prior to use. All experiments were performed under a nitrogen atmosphere using standard Schlenk techniques. ^{1}H NMR spectra were measured on a Bruker AVANCE 500 MHz spectrometer with tetramethylsilane as the internal standard. Mass spectra were recorded on a Shimadzu AXIMA-CFR MALDITOF mass spectrometer. Elemental analyses were performed on a flash EA 1112 spectrometer. UV-vis absorption spectra were recorded in CH_2Cl_2 (1×10^{-4} M) using a PE UV-vis lambdazo spectrometer. The emission spectra were recorded in CH_2Cl_2 (1×10^{-4} M) using Maya2000 Pro CCD spectrometer. The absolute fluorescence quantum yields in solution (1×10^{-4} M in CH_2Cl_2) and solid state were determined on Edinburgh FS920 steady state fluorimeter. Electrochemical measurements were performed with a BAS 100W Bioanalytical electrochemical work station, using Pt as working electrode, platinum wire as auxiliary electrode, and a porous glass wick Ag/Ag$^+$ as reference electrode, standardized against ferrocene/ferrocenium couple with a scan rate of 100 mV s^{-1}. Differential scanning calorimetric (DSC) measurements were performed on a NETZSCH DSC204 instrument. Thermogravimetric analyses (TGA) were performed on a TA Q500 thermogravimeter. 2,5-di(benzo[d]oxazol-2-yl)benzene-1,4-diol (**5**), 2,5-di(benzo[d]thiazol-2-yl)benzene-1,4-diol (**6**), 2-(benzo[d]oxazol-2-yl)phenol (**7**), 2-(benzo[d]thiazol-2-yl)phenol (**8**) were synthesized according to the literature procedures.[12]

Synthesis of complex 1. To a rapidly stirred solution of **5** (344 mg, 1.0 mmol) in THF (50 mL), BPh$_3$ (500 mg, 2.1 mmol) in THF (5 mL) was added and refluxed for 20 h. The volatiles were removed under vacuum, and the residual solid was purified by vacuum sublimation to give complex **1** as a red solid (200 mg, 30% yield). ^{1}H NMR (CDCl$_3$, ppm): δ 7.74 (d, $J = 8.5$ Hz, 2 H), 7.68 (s, 2 H), 7.49 (t, $J = 7.5$ Hz, 2 H), 7.42–7.40 (m, 8 H), 7.31 (t, $J = 7.5$ Hz, 2 H), 7.25–7.23 (m, 12 H), 7.00 (d, $J = 8.0$ Hz, 2 H). MS m/z: 671.8 [M]$^+$ (calcd: 672.2). Anal. calcd (%) for

$C_{44}H_{30}B_2N_2O_4$: C, 78.60; H, 4.50; N, 4.17; Found: C, 78.30; H, 4.50; N, 4.20.

Synthesis of complex 2. In the same manner as described for **1**, the reaction of **6** (540 mg, 1.44 mmol) and BPh$_3$ (765 mg, 3.16 mmol) provided **2** as a deep red solid (200 mg, 20% yield). ^{1}H NMR (CDCl$_3$, ppm): δ 7.92 (d, $J = 8.0$ Hz, 2 H), 7.46 (t, $J = 7.5$ Hz, 2 H), 7.39 (s, 2 H), 7.35–7.32 (m, 10 H), 7.29 (d, $J = 8.0$ Hz, 2 H), 7.22–7.21 (m, 12 H). MS m/z: 703.8 [M]$^+$ (calcd: 704.2). Anal. calcd (%) for $C_{44}H_{30}B_2N_2O_2S_2$: C, 75.02; H, 4.29; N, 3.98; S, 9.10; Found: C, 74.74; H, 4.32; N, 3.99; S, 8.97.

Synthesis of complex 3. In the same manner as described for **1**, the reaction of **7** (150 mg, 0.71 mmol) and BPh$_3$ (191 mg, 0.79 mmol) provided **3** as light yellow solid (157 mg, 59% yield). ^{1}H NMR (CDCl$_3$, ppm): δ 7.80 (dd, $J = 8.0$ Hz, 1.5 Hz, 1 H), 7.66 (d, $J = 8.5$ Hz, 1 H), 7.54–7.51 (m, 1 H), 7.44–7.40 (m, 5 H), 7.28–7.20 (m, 8 H), 6.99 (d, $J = 8.0$ Hz, 1 H), 6.90 (t, $J = 7.0$ Hz, 1 H). MS m/z: 374.5 [M]$^+$ (calcd: 375.1). Anal calcd (%) for $C_{25}H_{18}BNO_2$: C, 80.02; H, 4.84; N, 3.73; Found: C, 80.16; H, 4.73; N, 3.73.

Synthesis of complex 4. In the same manner as described for **1**, the reaction of **8** (110 mg, 0.48 mmol) and BPh$_3$ (120 mg, 0.50 mmol) provided **4** as light green solid (103 mg, 55% yield). ^{1}H NMR (CDCl$_3$, ppm): δ 7.87 (d, $J = 8.0$ Hz, 1 H), 7.52 (d, $J = 7.5$ Hz, 1 H), 7.45 (t, $J = 8.0$ Hz, 1 H), 7.41 (t, $J = 7.5$ Hz, 1 H), 7.38–7.36 (m, 4 H), 7.29–7.25 (m, 2 H), 7.24–7.21 (m, 6 H), 7.17 (d, $J = 8.0$ Hz, 1 H), 6.84 (t, $J = 8.0$ Hz 1 H). MS m/z: 390.1 [M]$^+$ (calcd: 390.1). Anal. calcd (%) for $C_{25}H_{18}BNOS$: C, 76.74; H, 4.64; N, 3.58; S, 8.19 Found: C, 76.77; H, 4.60; N, 3.60; S, 7.94.

Molecular orbital calculations

The ground state geometries were fully optimized by the density functional theory (DFT)[13] method with the Becke three-parameter hybrid exchange and the Lee–Yang–Parr correlation functional[14] (B3LYP) and 6-31G* basis set using the Gaussian 03 software package.[15]

Electroluminescent properties

The general architecture of the complex multilayer diodes used in this study is as follows: Indium–tin oxide (ITO) coated glass was used as the substrate. It was cleaned by sonication successively in a detergent solution, acetone, methanol, and deionized water before use. All organics, including N,N'-di(1-naphthyl)-N,N'-diphenyl-(1,1'-biphenyl)-4,4'-diamine (NPB), 4,4'-bis(2,2-diphenylvinyl)-1,1'-biphenyl (DPVBi), 4,4',4''-tris(carbazol-9-yl)triphenylamine (TCTA) and 4,7-diphenyl-1,10-phenanthroline (Bphen) were purified by gradient sublimation and thermally evaporated at a rate of 1.0 Å s^{-1} at a base pressure of around 3.5 $\times 10^{-4}$ Pa. After the organic film deposition, LiF and aluminum were thermally evaporated onto the organic surface. The thicknesses of the organic materials and the cathode layers were controlled using a quartz crystal thickness monitor. The electrical characteristics of the devices were measured with a Keithley 2400 source meter. The EL spectra and luminance of the devices were obtained on a PR650 spectrometer.

This journal is © The Royal Society of Chemistry 2011

J. Mater. Chem., 2011, **21**, 15298–15304 | 15299

Crystal data

Diffraction data were collected on a Rigaku RAXIS-PRID diffractometer using the ω-scan mode with graphite-monochromator Mo•Kα radiation. The structures were solved with direct methods using the SHELXTL programs[16] and refined with full-matrix least-squares on F^2. Non-hydrogen atoms were refined anisotropically. The positions of hydrogen atoms were calculated and refined isotropically.

Results and discussion

Synthesis and characterization

Scheme 1 outlines the synthetic route to diboron-contained seven-ring fused complexes **1** and **2**, together with that to the reference monoboron-containing four-ring fused complexes **3** and **4**, which were synthesized for the purpose of property comparison. Simple mixing of the ligands and triphenyl borane in THF under reflux conditions and subsequent purification by vacuum sublimation produced targets **1–4** in moderate yields (20–59%), which were fully characterized by ^{1}H NMR, mass spectra, element analyses and finally confirmed by X-ray crystal analysis.

Crystal structures

Single crystals of **1** and **2** were obtained by vacuum sublimation and their structures were determined by X-ray crystallography. The crystal lattices of **1** and **2** are both centrosymmetric and belong to the triclinic P_{-1} space group. All boron atoms adopt a typical tetrahedral geometry to form N,O-chelate six-membered rings, which contribute to constructing the seven-ring fused π-conjugated skeletons (Fig. 1a and b). In both crystals, the six-membered rings constructed by boron chelation take a chair conformation in which the oxygen and boron atoms deviate from the central phenyl plane by 0.07 Å and 0.59 Å for **1** and 0.10 Å and 0.47 Å for **2** in opposite directions. The bond lengths of B–N, B–O and B–C are 1.63 Å, 1.51 Å, 1.60 Å for **1** and 1.66 Å, 1.50 Å, 1.61 Å for **2**, which are similar to those of the organoboron compounds previously reported.[10] The dihedral angle between the outer benzo[d]oxazole/benzo[d]thiazole plane and the central benzene ring is 13.1° in **1** and 12.8° in **2**, indicating
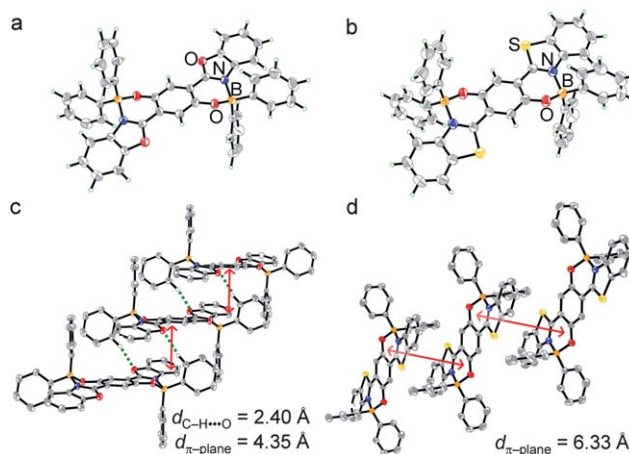

Fig. 1 Molecular structures of **1** (a) and **2** (b) with 50% thermal ellipsoids and packing structures of **1** (c) and **2** (d).

that the π-systems have certain distortions from the coplanar framework. Although crystals **1** and **2** have identical molecular structures, their packing modes are quite different. In **1**, molecules packed into a one-dimensional column by face-to-face π–π interaction with an interfacial distance of 4.35 Å, which was further stabilized by C–H⋯O hydrogen bonds, as shown in Fig. 1c. There are no obvious π–π interactions in the packing structure of **2**, and the distance between neighboring π-conjugated planes is 6.33 Å, which is far from the distance range of π–π interaction (Fig. 1d).

Photophysical properties

The absorption and fluorescence properties of **1** and **2** in both solution and the solid state, together with those of reference **3** and **4**, were tested. The data are summarized in Table 1 and the spectra are shown in Fig. 2 and 3. The absolute fluorescence quantum yields (Φ_f) of solutions and solids are all determined using an integrating sphere.

As depicted in Fig. 2 and 3, complex **3** exhibits blue fluorescence with an emission band peaked at 452 nm ($\Phi_f = 0.55$) in dichloromethane (CH$_2$Cl$_2$) and 462 nm ($\Phi_f = 0.53$) in the solid state. Complex **4** is bluish green fluorescent with an emission band centred at 485 nm ($\Phi_f = 0.65$) in CH$_2$Cl$_2$ and 494 nm ($\Phi_f = 0.60$) in the solid state. The fluorescence efficiencies of BPh$_2$-chelate complexes are greatly improved compared to those of the BF$_2$-chelate analogs (0.20 and 0.23 in CH$_2$Cl$_2$) based on the same ligands, presumably due to the large steric hindrance of the diphenyl boron chelation, which can effectively prevent molecular aggregation. The seven-ring fused diboron complexes **1** and **2** are red fluorescent with the absorption maximum of 491 nm and emission band centred at 610 nm ($\Phi_f = 0.55$) in dichloromethane (CH$_2$Cl$_2$) for **1** and the absorption maximum of 515 nm and emission band centred at 660 nm ($\Phi_f = 0.34$) in dichloromethane for **2**. Comparing with the four-ring fused monoboron complexes, the longest absorption (491 nm) and emission (610 nm) maxima of **1** in CH$_2$Cl$_2$ are significantly redshifted by 122 and 158 nm from those of complex **3** ($\lambda_{abs} = 369$ nm; $\lambda_{em} = 452$ nm), and similarly, the longest absorption (515 nm) and emission (660 nm) maxima of **2** in CH$_2$Cl$_2$ are redshifted by 126 and 175
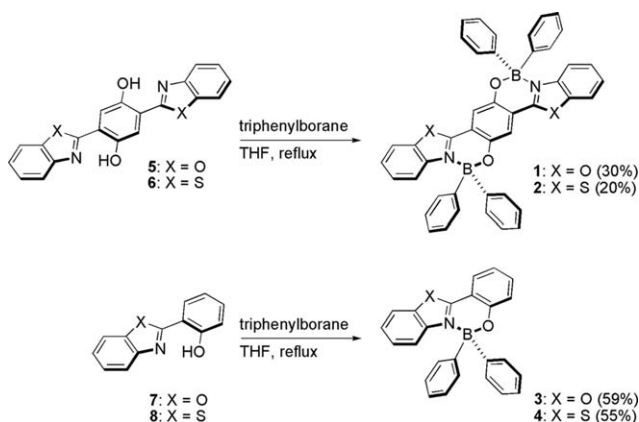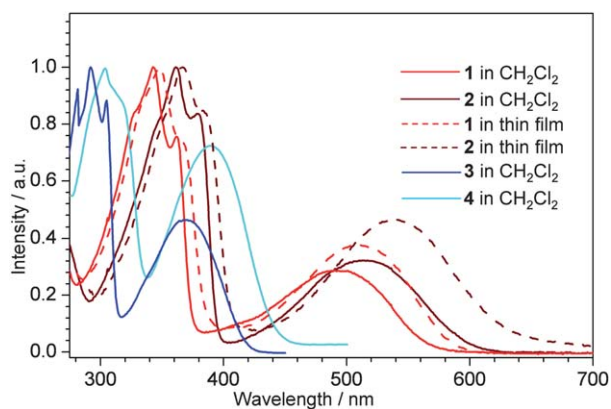

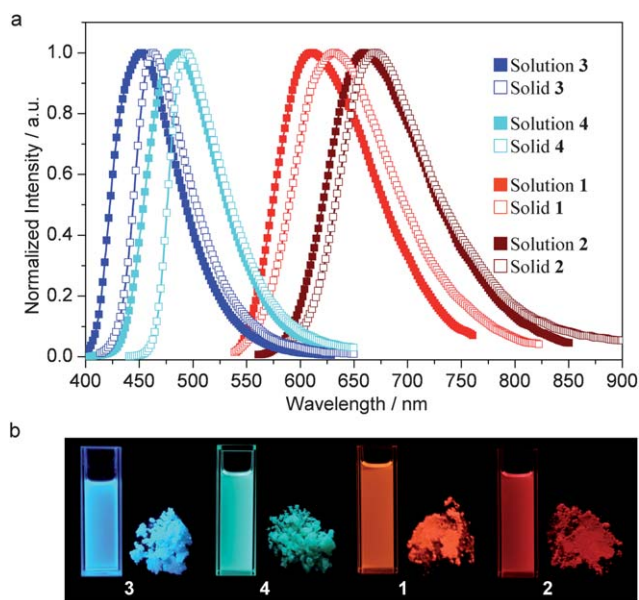**Scheme 1** Synthetic routes to the boron complexes **1–4**.

Table 1 Photophysical properties of complexes **1–4**

compound	λ_{abs} (nm)[a,b] (logε)	λ_{em} (nm)		Φ_f	
		solution[a]	powder	solution[a]	powder
1	491 (4.18)	610	632	0.55	0.30
2	515 (4.24)	660	670	0.34	0.41
3	369 (4.15)	452	462	0.55	0.53
4	389 (4.09)	485	494	0.65	0.60

[a] Data were collected in CH_2Cl_2 (1×10^{-4} M). [b] Only the longest absorption maxima are shown.

Fig. 2 UV-Vis absorption spectra of complexes **1–4** in CH_2Cl_2 (solid line) and those of **1** and **2** in thin film (dash line).

Fig. 3 Emission spectra (a) and photographs under UV light ($\lambda_{ex} = 365$ nm) (b) of **1–4** in CH_2Cl_2 and the solid state.

complex **1**, due to the heavy atom effect. In the solid state, the longest absorption and emission maxima are 508 nm and 632 nm for **1** and 539 nm and 670 nm for **2**. The emission of **1** in the solid state (632 nm) is redshifted by 22 nm compared to that in solution (610 nm), accompanied by Φ_f decreasing from 0.55 to 0.30, due to the presence of π–π interactions between luminescent skeletons as observed in crystal packing structure. Notably, CH_2Cl_2 solution (660 nm) and solid (670 nm) of complex **2** don't show significant difference in fluorescence spectra, and the solid exhibits even higher fluorescence quantum yield ($\Phi_f = 0.41$) compared to the solution ($\Phi_f = 0.34$). The enhanced fluorescence efficiency of solid **2** can be explained by its crystal structure feature, namely, side phenyl groups prevent π–π interactions between luminescent skeletons, and the rigid framework effectively restrict molecular rotations. Both red fluorophores don't suffer from serious fluorescence quenching in the solid state. This observation reflects that the four side phenyl groups attached to boron atoms are effective in keeping the luminescent unit apart, consistent with the crystal structure analysis.

Electrochemical properties and molecular orbital calculations

The electrochemical properties of boron complexes **1–4** were characterized by cyclic voltammetry. Their cyclic voltammograms are shown in Fig. 4 and the data are summarized in Table 2. The monoboron complexes display a irreversible reduction wave with peak potential (E_{pc}) at −2.28 V for **3** and a quasi-reversible reduction wave with reduction potential $E_{red}^{1/2}$ at
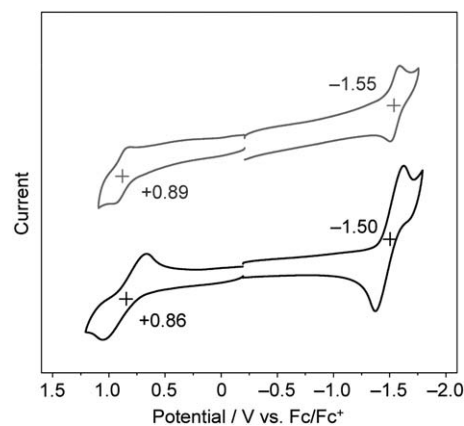
Fig. 4 (a) Cyclic voltammograms of **1** (gray line) and **2** (black line) in CH_2Cl_2 (oxidation, 1 mM) and THF (reduction, 1 mM), measured with TBAP (0.1 M) as a supporting electrolyte at a scan rate of 100 mV s^{-1}.

nm from those of complex **4** ($\lambda_{abs} = 389$ nm; $\lambda_{em} = 485$ nm), which reflects the great influence of the extended π-conjugation on optical properties.

In CH_2Cl_2, the absorption and emission maxima of the benzo[d]thiazole fused complex **2** are redshifted by about 24 and 50 nm, respectively, compared to those of the benzo[d]oxazole fused

This journal is © The Royal Society of Chemistry 2011

*J. Mater. Chem.*, 2011, **21**, 15298–15304 | **15301**

Table 2 Electrochemical data[a] of complexes **1–4**

compound	$E_{\text{ox}}^{1/2}$ (V)[b]	ΔE_{ox} (V)	$E_{\text{red}}^{1/2}$ (V)[c]	ΔE_{red} (V)
1	+0.89	0.10	−1.55	0.09
2	+0.86	0.40	−1.50	0.26
3	+1.17[d]	[e]	−2.28[d]	[e]
4	+1.11[d]	[e]	−2.22	0.27

[a] Potentials are given against ferrocene/ferrocenium (Fc/Fc+). [b] Measured in CH_2Cl_2. [c] Measured in THF. [d] Peak potential. [e] Not observed.

−2.22 V for **4**. Complexes **1** and **2** show reversible and quasi-reversible one-electron reduction waves with the reduction potentials ($E_{\text{red}}^{1/2}$) of −1.55 and −1.50 V, respectively. Both of the diboron complexes **1** and **2** have large positively shifted reduction waves compared with the monoboron complexes **3** and **4**. This result demonstrates that extension of the π-system from monoboron to diboron not only makes the cathodic reductions easier but also stabilizes the radical anions produced. Moreover, the reduction potentials of **1** and **2** are positively shifted by 0.75 and 0.80 V compared to that of Alq3 (E_{pc} = −2.3 V), one of the most widely used electron-transporting materials, demonstrating the high electron-accepting ability of these boron complexes. Notably, **1** and **2** also show reversible and quasi-reversible oxidation waves with $E_{\text{ox}}^{1/2}$ = +0.89 and +0.86 V, respectively, which are negatively shifted by 0.28 and 0.25 V compared with that of **3** (E_{pa} = +1.17 V) and **4** (E_{pa} = +1.11 V). On the basis of the oxidation and reduction potentials, the highest occupied molecular orbitals (HOMO) and lowest unoccupied molecular orbitals (LUMO) energy levels are calculated to be −5.69 and −3.25 eV for **1**, −5.66 and −3.30 eV for **2**, −5.97 and −2.52 eV for **3** and −5.91 and −2.58 eV for **4**.

To obtain a deeper insight into the electronic structures of these π-systems, density functional theory (DFT) calculations at the B3LYP/6-31G(d) level were carried out. The electronic structures are identical between **1** and **2**, as well as **3** and **4**, therefore, only the molecular orbital diagrams of complexes **1** and **3** are presented in Fig. 5. As for the monoboron complexes, both HOMOs and LUMOs are delocalized on the entire four-ring-fused skeleton. The HOMO levels are almost the same, being −5.87 eV for **3** and −5.86 eV for **4**, while the LUMO levels
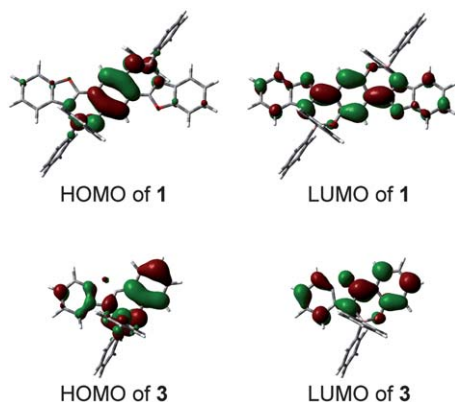
Fig. 5 Molecular orbital diagrams for HOMOs and LUMOs of **1** and **3**.

of −2.01 eV for **3** and −2.20 eV for **4** show a certain difference, demonstrating that modulation of bridging atoms mainly influences the LUMO level. The HOMOs of diboron complexes are localized on the central benzene ring and the chelated O–B–N moieties, and the LUMOs are delocalized on the entire π-conjugated skeleton. Diboron complexes **1** and **2** also have similar HOMO levels (−5.53 eV for **1** and −5.51 eV for **2**) but different LUMO levels (−2.80 eV for **1** and −2.90 eV for **2**). A comparison of energy levels between monoboron and diboron complexes reveals that the π-conjugation extension can push the HOMO level up and meanwhile pull the LUMO level down, hence significantly narrowing the bandgap of the extended π-system. Although HOMOs and LUMOs of **1** and **2** reside on different parts of the molecules, no intramolecular charge transfer takes place considering the fact that both complexes keep the emission profile identical when increasing the solvent polarity from toluene to dichloromethane and finally to acetonitrile (Fig. S2†).

Thermal analyses

The thermal properties of **1** and **2** were characterized by thermogravimetric analysis (TGA) and differential scanning calorimetry (DSC) under a nitrogen atmosphere at a heating rate of 10 °C min⁻¹. Fig. S3 shows the DSC and TGA curves of complexes **1** and **2**.† Both diboron complexes are thermally stable as evidenced by their high melting points (432 °C for **1** and 431 °C for **2**) and decomposition temperatures (5% weight loss temperature located at 406 °C for **1** and 416 °C for **2**), which ensures them to be stable for vacuum evaporation in OLEDs.

Electron mobility

To further affirm the electron transport ability, time of flight (TOF) carrier-mobility measurement based on complexes **1** and **2** with device configuration of ITO/complexes **1** or **2** (1–2 μm)/Al was carried out at room temperature. Fig. 6 displays typical TOF transients of electrons for complexes **1** and **2** under an applied field. The transient photocurrent signals were dispersive, suggesting the presence of electron traps. According to the equation $\mu = D/ET_t$, where D is the thickness of the transporting layer, E is the electrical field strength, the electron mobilities of the vacuum-deposited films were determined to be 7.7×10^{-4} cm² V⁻¹ s⁻¹ for **1** and 2.2×10^{-4} cm² V⁻¹ s⁻¹ for **2**. These mobility values are comparable to that of diboron-contained thienylthiazoles (Scheme 2) which have similar extended π-conjugated planar skeleton ($\mu_e = 1.5 \times 10^{-4}$ cm² V⁻¹ s⁻¹ measured by means of the TOF method).[17]

Electroluminescent properties

Considering the intense luminescence, good thermal stability, as well as high electron mobility of these boron solids, OLED devices with configuration of ITO/NPB (35 nm)/DPVBi (2 nm) for **1** and TCTA (2 nm) for **2**/**1** or **2** (60 nm)/Bphen (3 nm)/LiF (0.5 nm)/Al (200 nm) were fabricated by multi-layer vapour deposition to briefly evaluate the potential of these boron complexes used as electron-transporting red emitting materials. As shown in Fig. 7 and 8, the EL device fabricated by complex **1** exhibited a pure red electroluminescence peaked at 628 nm with
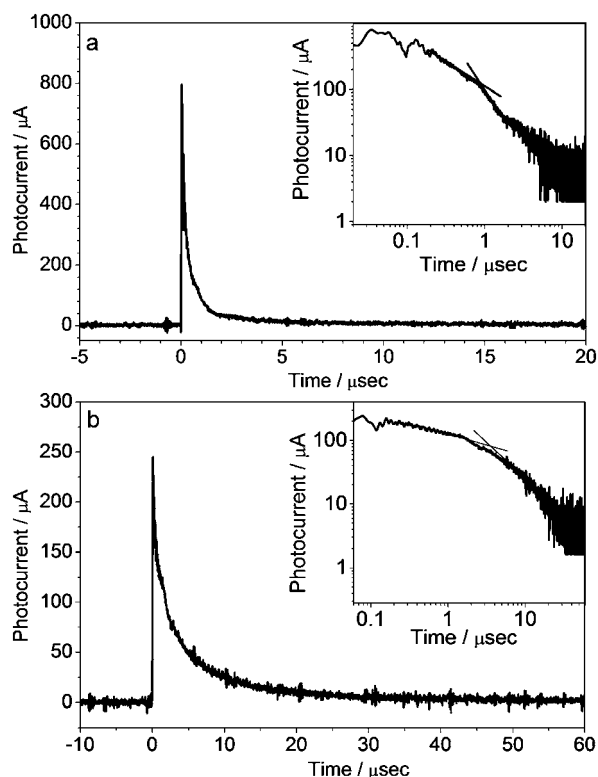
Fig. 6 TOF transients for electrons at room temperature: (a) complex **1**, $D = 3.10$ μm, $E = 4.52 \times 10^5$ V cm^{-1} and $T_t = 0.89$ μs; (b) complex **2**, $D = 2.78$ μm, $E = 3.60 \times 10^5$ V cm^{-1} and $T_t = 3.56$ μs. Insets: Double logarithmic plots of data in (a) and (b).
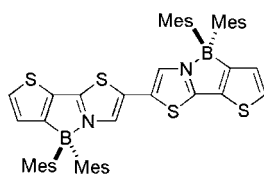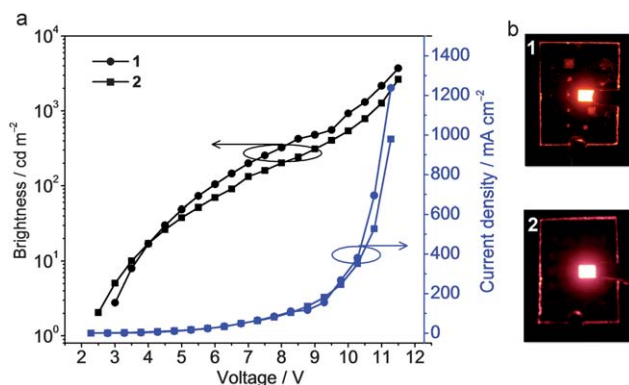
Scheme 2 The molecular structure of diboron-contained thienylthiazole.
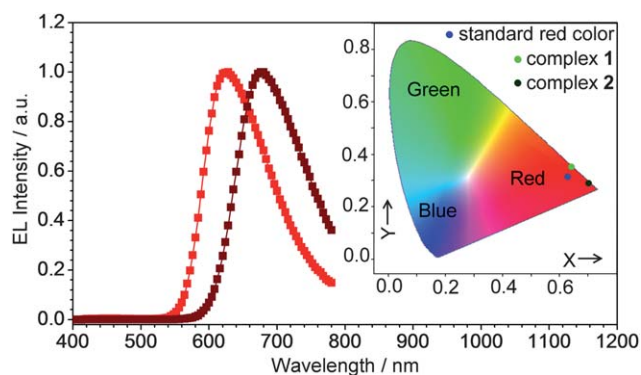
Fig. 7 The electroluminescence spectra for **1** and **2**. Inset: CIE chromaticity diagrams of devices.

CIE coordinates of ($X = 0.64$; $Y = 0.36$). It turned on at a very low voltage of 2.5 V and reached a maximum brightness of 3704 cd m^{-2} and a maximum power efficiency of 0.53 lm W^{-1}. The

Fig. 8 (a) Current density–brightness–voltage characteristics of devices of complexes **1** and **2**. (b) Photographic images of devices.

OLED device employing **2** as an electron-transporting emitter showed strong red to near infrared electroluminescence peaked at 680 nm with CIE coordinates of ($X = 0.70$; $Y = 0.30$), a turn on voltage of 3.0 V, a maximum brightness of 2636 cd m^{-2}, and a maximum power efficiency of 0.46 lm W^{-1}. Notably, the practical maximum brightness of device based on **2** should be higher than the detected value due to the significant missed proportion of the emission appearing in the near-IR region, as shown in Fig. 7. Taking into account the deep red EL spectra of complexes **1** and **2**, as well as their other favourable characteristics introduced in this paper, we believe it is worthwhile to further optimize the device fabrication for higher performance.

Conclusions

In conclusion, two brightly fluorescent red solids bearing extended π-conjugated skeletons have been synthesized. The rigid seven-ring fused core structure bridged by boron atoms endows these compounds with high electron mobility and good thermal stability. In addition, two side phenyl groups coordinated to each boron atom effectively keep the luminescent units apart. As a result, these red fluorophores are brightly fluorescent in the solid state. These favourable characteristics enable them to be suitable candidates for non-doped red emitters with an excellent electron-transporting nature in electroluminescent devices.

Acknowledgements

Notes and references

1 (a) Y. Kim, J. Bouffard, S. E. Kooi and T. M. Swager, *J. Am. Chem. Soc.*, 2005, **127**, 13726; (b) A. Wakamiya, K. Mori and S. Yamaguchi, *Angew. Chem., Int. Ed.*, 2007, **46**, 4273; (c) S. Ye, J. Chen, C. Di, Y. Liu, K. Lu, W. Wu, C. Du, Y. Liu, Z. Shuai and G. Yu, *J. Mater. Chem.*, 2010, **20**, 3186.
2 (a) Y.-S. Yao, Q.-Z. Zhou, X.-S. Wang, Y. Wang and B.-W. Zhang, *J. Mater. Chem.*, 2006, **16**, 3512; (b) S. A. Odom, S. R. Parkin and J. E. Anthony, *Org. Lett.*, 2003, **5**, 4245.
3 (a) A. Craft, A. C. Grimsdale and A. B. Holmes, *Angew. Chem., Int. Ed.*, 1998, **37**, 402; (b) M. D. Watson, A. Fechtenkötter and

This journal is © The Royal Society of Chemistry 2011

J. Mater. Chem., 2011, **21**, 15298–15304 | 15303

K. Müllen, *Chem. Rev.*, 2001, **101**, 1267; (*c*) J. E. Anthony, *Angew. Chem., Int. Ed.*, 2008, **47**, 452; (*d*) U. Scherf, *J. Mater. Chem.*, 1999, **9**, 1853.

4 (*a*) S. Yamaguchi, C. Xu and K. Tamao, *J. Am. Chem. Soc.*, 2003, **125**, 13662; (*b*) C. Xu, A. Wakamiya and S. Yamaguchi, *J. Am. Chem. Soc.*, 2005, **127**, 1638; (*c*) A. Fukazawa, H. Yamada and S. Yamaguchi, *Angew. Chem., Int. Ed.*, 2008, **47**, 5582; (*d*) H. Tian, Y. Deng, F. Pan, L. Huang, D. Yan, Y. Geng and F. Wang, *J. Mater. Chem.*, 2010, **20**, 7998; (*e*) R. K. Cheedarala, G.-H. Kim, S. Cho, J. Lee, J. Y. Kim and C. Yang, *J. Mater. Chem.*, 2011, **21**, 843.

5 (*a*) Q. Wu, M. Esteghamatian, N.-X. Hu, Z. Popovic, G. Enright, Y. Tao, M. Diorio and S. Wang, *Chem. Mater.*, 2000, **12**, 79; (*b*) Q. Liu, M. S. Mudadu, H. Schmider, R. Thummel, Y. Tao and S. Wang, *Organometallics*, 2002, **21**, 4743; (*c*) Y. Cui, Q.-D. Liu, D.-R. Bai, W.-L. Jia, Y. Tao and S. Wang, *Inorg. Chem.*, 2005, **44**, 601; (*d*) Q.-D. Liu, M. S. Mudadu, R. Thummel, Y. Tao and S. Wang, *Adv. Funct. Mater.*, 2005, **15**, 143.

6 (*a*) S. L. Hellstrom, J. Ugolotti, G. J. P. Britovsek, T. S. Jones and A. J. P. White, *New J. Chem.*, 2008, **32**, 1379; (*b*) J. Ugolotti, S. Hellstrom, G. J. P. Britovsek, T. S. Jones, P. Hunt and A. J. P. White, *Dalton Trans.*, 2007, **14**, 1425; (*c*) H.-Y. Chen, Y. Chi, C.-S. Liu, J.-K. Yu, K.-M. Cheng, K.-S. Chen, P.-T. Chou, S.-M. Peng, G.-H. Lee, A. J. Carty, S.-J. Yeh and C.-T. Chen, *Adv. Funct. Mater.*, 2005, **15**, 567; (*d*) T.-R. Chen, R.-H. Chien, M.-S. Jan, A. Yeh and J.-D. Chen, *J. Organomet. Chem.*, 2006, **691**, 799; (*e*) S. Kappaun, S. Rentenberger, A. Pogantsch, E. Zojer, K. Mereiter, G. Trimmel, R. Saf, K. C. Möller, F. Stelzer and C. Slugovc, *Chem. Mater.*, 2006, **18**, 3539; (*f*) T.-R. Chen, R.-H. Chien, A. Yeh and J.-D. Chen, *J. Organomet. Chem.*, 2006, **691**, 1998.

7 (*a*) Y. Qin, I. Kiburu, S. Shah and F. Jäkle, *Macromolecules*, 2006, **39**, 9041; (*b*) Y. Qin, I. Kiburu, S. Shah and F. Jäkle, *Org. Lett.*, 2006, **8**, 5227; (*c*) Y. Qin, C. Pagba, P. Piotrowiak and F. Jäkle, *J. Am. Chem. Soc.*, 2004, **126**, 7015; (*d*) F. Cheng and F. Jäkle, *Chem. Commun.*, 2010, **46**, 3717; (*e*) S. F. Liu, Q. Wu, H. L. Schmider, H. Aziz, N.-X. Hu, Z. Popović and S. Wang, *J. Am. Chem. Soc.*, 2000, **122**, 3671; (*f*) Y. L. Rao, H. S. Amarne, B. Zhao, T. M. McCormick, S. Martić, Y. Sun, R. Y. Wang and S. Wang, *J. Am. Chem. Soc.*, 2008, **130**, 12898; (*g*) C. Baik, Z. M. Hudson, H. Amarne and S. Wang, *J. Am. Chem. Soc.*, 2009, **131**, 14549.

8 (*a*) Y. Li, Y. Liu, W. Bu, J. Guo and Y. Wang, *Chem. Commun.*, 2000, 1551; (*b*) J. Feng, F. Li, W. B. Gao, S. Y. Liu, Y. Liu and Y. Wang, *Appl. Phys. Lett.*, 2001, **78**, 3479; (*c*) Y. Liu, J. Guo, H. Zhang and Y. Wang, *Angew. Chem., Int. Ed.*, 2002, **41**, 182; (*d*) H. Zhang, C. Huo, K. Ye, P. Zhang, W. Tian and Y. Wang, *Inorg. Chem.*, 2006, **45**, 2788; (*e*) H. Zhang, C. Huo, J. Zhang, P. Zhang, W. Tian and Y. Wang, *Chem. Commun.*, 2006, 281; (*f*) Z. Zhang, D. Yao, S. Zhao, H. Gao, Y. Fan, Z. Su, H. Zhang and Y. Wang, *Dalton Trans.*, 2010, **39**, 5123.

9 Q. Zhao, H. Zhang, A. Wakamiya and S. Yamaguchi, *Synthesis*, 2009, 127.

10 (*a*) Z. L. Zhang, H. Bi, Y. Zhang, D. D. Yao, H. Z. Gao, Y. Fan, H. Y. Zhang, Y. Wang, Y. P. Wang, Z. Y. Chen and D. G. Ma, *Inorg. Chem.*, 2009, **48**, 7230; (*b*) D. Li, Z. Zhang, S. Zhao, Y. Wang and H. Zhang, *Dalton Trans.*, 2011, **40**, 1279; (*c*) D. Li, Y. Yuan, H. Bi, D. D. Yao, X. J. Zhao, W. J. Tian, Y. Wang and H. Y. Zhang, *Inorg. Chem.*, 2011, **50**, 4825.

11 M. J. Kwak and Y. Kim, *Bull. Korean Chem. Soc.*, 2009, **30**, 2865.

12 (*a*) A. Mordziński, A. Grabowska, W. Kühnle and A. Kröwczyński, *Chem. Phys. Lett.*, 1983, **101**, 291; (*b*) N. P. Ernsting, A. Mordzinski and B. Dick, *J. Phys. Chem.*, 1987, **91**, 1404.

13 E. Runge and E. K. U. Gross, *Phys. Rev. Lett.*, 1984, **52**, 997.

14 A. D. J. Becke, *Chem. Phys.*, 1993, **98**, 5648.

15 M. J. Frisch, G. W. Trucks, H. B. Schlegel, G. E. Scuseria, M. A. Robb, J. R. Cheeseman, J. A. Montgomery, Jr., T. Vreven, K. N. Kudin, J. C. Burant, J. M. Millam, S. S. Iyengar, J. Tomasi, V. Barone, B. Mennucci, M. Cossi, G. Scalmani, N. Rega, G. A. Petersson, H. Nakatsuji, M. Hada, M. Ehara, K. Toyota, R. Fukuda, J. Hasegawa, M. Ishida, T. Nakajima, Y. Honda, O. Kitao, H. Nakai, M. Klene, X. Li, J. E. Knox, H. P. Hratchian, J. B. Cross, C. Adamo, J. Jaramillo, R. Gomperts, R. E. Stratmann, O. Yazyev, A. J. Austin, R. Cammi, C. Pomelli, J. W. Ochterski, P. Y. Ayala, K. Morokuma, G. A. Voth, P. Salvador, J. J. Dannenberg, V. G. Zakrzewski, S. Dapprich, A. D. Daniels, M. C. Strain, O. Farkas, D. K. Malick, A. D. Rabuck, K. Raghavachari, J. B. Foresman, J. V. Ortiz, Q. Cui, A. G. Baboul, S. Clifford, J. Cioslowski, B. B. Stefanov, G. Liu, A. Liashenko, P. Piskorz, I. Komaromi, R. L. Martin, D. J. Fox, T. Keith, M. A. Al-Laham, C. Y. Peng, A. Nanayakkara, M. Challacombe, P. M. W. Gill, B. Johnson, W. Chen, M. W. Wong, C. Gonzalez, J. A. Pople, *Gaussian 03, Revision C.02*, Gaussian, Inc., Pittsburgh, PA 2003.

16 *SHELXTL*, Version 5.1; Siemens Industrial Automation, Inc. 1997; G. M. Sheldrick, *SHELXS-97, Program for Crystal Structure Solution*, University of Göttingen, Göttingen, 1997.

17 A. Wakamiya, T. Taniguchi and S. Yamaguchi, *Angew. Chem., Int. Ed.*, 2006, **45**, 3170.